WKB study of fluctuations and activation in nonequilibrium dissipative steady states

R. Kupferman
School of Physics and Astronomy, Raymond and Beverly Sackler Faculty of Exact Sciences, Tel-Aviv University, Ramat-Aviv, Tel-Aviv 69978, Israel

M. Kaiser and Z. Schuss
School of Mathematics, Raymond and Beverly Sackler Faculty of Exact Sciences, Tel-Aviv University, Ramat-Aviv, Tel-Aviv 69978, Israel

E. Ben-Jacob
School of Physics and Astronomy, Raymond and Beverly Sackler Faculty of Exact Sciences, Tel-Aviv University, Ramat-Aviv, Tel-Aviv 69978, Israel

(Received 21 June 1991)

We present analytical and numerical studies of fluctuations about and transitions from the nonequilibrium dissipative steady state to the stable equilibrium state of a damped physical pendulum driven by constant torque and small white noise. We find the probability density function of the local flucutations about the nonequilibrium steady state and the transition rate from the nonequilibrium state to the equilibrium state by constructing an asymptotic solution to the Fokker-Planck equation by the WKB method. The solution to the eikonal (Hamilton-Jacobi) equation is constructed both analytically by an asymptotic series expansion, and numerically by integrating the set of characteristic equations. We compare the numerical results to the analytical calculations and determine the limits of validity of the asymptotic approximation. We apply the results to the case of the hysteretic Josephson junction and discuss a generalization of the numerical and analytical methods to other systems.

PACS number(s): 34.10.+x, 85.25.Dq, 85.25.Cp

I. INTRODUCTION

Today, fifty years after the classical paper of Kramers [1], the problem of thermal activation from a potential well is well understood. According to this theory the transition rate of a one-dimensional Brownian particle over a potential barrier is given by

$$\kappa=\Omega e^{-\Delta U/k_B T}, \tag{1.1}$$

where ΔU is the height of the potential barrier, T is the temperature of a heat bath coupled to the system, and k_B is Boltzmann's constant. The so-called attempt frequency Ω is proportional to the dissipation parameter in the limit of weak damping and inversely proportional to it in the limit of strong damping. The exponential dependence on $\Delta U/k_B T$ is a direct consequence of the Boltzmann distribution of fluctuations about the stable equilibrium state at the bottom of the potential well. Kramers's result (1.1) has since been extended to multidimensional systems [2,3] and to include general noises, such as colored noise and state-dependent noise. Explicit expressions for the attempt frequency Ω have been derived for many different systems, including systems with and without detailed balance (see, e.g., [4]–[14]). The activation problem was also considered for quantum systems, where the potential barrier can be breached both by tunneling across the barrier and by thermal activation over the barrier [15]. In parallel with theoretical developments, the activation problem from a potential well was the subject of extensive experimental studies in various systems and excellent agreement with theory was found [16,17].

An equally important problem is that of fluctuations about and transition rates from a nonequilibrium steady state to a stable equilibrium state in hysteretic multistable systems. The recent interest stems from the study of the voltage state of the shunted hysteretic Josephson [18,19]. The theoretical treatment of this problem started less than a decade ago with the pioneering work of Risken and Vollmer [20], followed by Ben-Jacob *et al.* [21] and more recently by Graham and Tél [22], and yet there is no generally accepted analytical theory of this problem.

The canonical example used for the study of hysteretic multistable systems is the damped physical pendulum, forced by constant torque and small white noise. It serves as a model for various physical systems, including the shunted hysteretic Josephson junction [23,24], charge-density waves [25], power systems [26], and phase-locked loops [27], to name but a few. Indeed, the order parameters in the Josephson junction obeys the same nondimensional equations as that of the noise physical pendulum

$$\ddot{\theta}+G\dot{\theta}+\sin\theta=I+L(t), \tag{1.2}$$

where the superconducting phase difference θ, the superconducting coupling $\sin\theta$, the nondimensional driving current I, and the nondimensional Ohmic resistance G of the shunt resistor correspond to the angle, gravitational force, external torque, and dissipation of the pendulum, respectively. The function $L(t)$ represents the noise in the system.

The common property of these different systems is the coexistence of two qualitatively different stable steady states: a stable equilibrium state and a stable dissipative nonequilibrium steady-state, a periodic limit curve S in phase space (Fig. 2) [21,28,29]. The nonequilibrium steady state in the context of the pendulum corresponds to a rotational motion of the pendulum. It can also be viewed as a model of a particle sliding down a washboard potential (Fig. 1) and is therefore also referred to as the running state. For the shunted Josephson junction the stable equilibrium state corresponds to the zero voltage state of the junction, whereas the nonequilibrium steady state corresponds to its voltage state [21]. Due to the presence of the thermal noise $L(t)$ the system fluctuates about the stable equilibrium state or the nonequilibrium steady state with occasional noise-induced transitions between the two.

Small fluctuations about the stable equilibrium state are described well by the Boltzmann distribution so that their structure is well understood. Noise-induced transitions from the stable equilibrium state to the nonequilibrium steady state are identical to the escape of a Brownian particle over a potential barrier and are accurately described by Kramers's theory of activation.

To calculate the probability density function of the fluctuations about the nonequilibrium steady state, various numerical methods have been developed [7,14]. Ben-Jacob *et al.* [21] have developed an asymptotic approach to the analytical calculation of the probability density function of the fluctuations and the transition rates in the limit of weak damping (a review is presented in Sec. III). It was shown in [21] that the steady-state probability density function $\rho(\dot{\theta},\theta)$ in phase space is given by

$$\rho(\dot{\theta},\theta)=\rho_0 e^{-W(\theta,\dot{\theta})/k_B T}, \tag{1.3}$$

where $W(\theta,\dot{\theta})$ is the effective energy. It can be expressed by means of an action variable $A(\theta,\dot{\theta})$ as

$$W(\theta,\dot{\theta})=\tfrac{1}{2}[A(\theta,\dot{\theta})-A_0]^2, \tag{1.4}$$

where A_0 is the action of the limit curve S. It was shown that through each point $(\theta,\dot{\theta})$ in the basin of attraction of the nonequilibrium steady state passes a unique steady-state phase-space trajectory S_Γ of a junction with a certain value $\Gamma(\theta,\dot{\theta})$ of the damping parameter G. For $(\theta,\dot{\theta})$ above S we have $\Gamma(\theta,\dot{\theta})<G$ and the reverse inequality holds below S (Fig. 4). The action $A(\theta,\dot{\theta})$ is calculated on one period of S_Γ. The transition rate from the nonequilibrium steady state to the stable equilibrium state was shown to be

$$\kappa=\Omega e^{-\Delta W/k_B T}, \tag{1.5}$$

where the effective barrier height ΔW is given by $\Delta W=\frac{1}{2}(A_0-A_c)^2$ with A_c the action of the critical first trajectory S_Γ that touches the separatrix between the basins of attraction of the nonequilibrium steady state and of the stable equilibrium state (Figs. 8 and 9). This analytical method has been extended to the case of a Josephson junction in the presence of microwave radiation [30], a dc-SQUID (where SQUID denotes "superconducting quantum interference device") (two coupled junctions) [31], shot noise instead of thermal noise [32], and to a system described by a master equation rather than by the Fokker-Planck equation [33]. Recently the transition rate from the voltage state of a hysteric Josephson junction was measured [18,19] and excellent agreement with the theoretical results of [21] was found.

Yet, the range of the validity of the analytical results of [21] has been called into question [22]. The purpose of the present paper is to study the nonequilibrium steady state both analytically and numerically and to establish the range of validity of the asymptotic expansion presented in [21]. The main results of this paper follow. (i) The W contours coincide very well with the steady-state trajectories. A typical maximal deviation for $W\approx\frac{1}{2}\Delta W$ is less than 1%. (ii) As I approaches the critical value 1, the analytical approximation breaks down for a reason explained in Sec. V. (iii) The approximation for ΔW is very accurate in a wide range of values of I. For $G=0.15$, even for $I=0.8$ the error is less than 2% (the error is much smaller for lower values of I). For $G=0.5$ the error is about 10% for $I=0.8$. We emphasize that for large values of I the nonequilibrium steady state is much more stable than the stable equilibrium state (see Sec. VI), thus this range is of little practical interest as no transitions from the nonequilibrium steady state can be observed.

In Sec. II we review the dynamics of an underdamped physical pendulum in the absence of noise and in Sec. III we review the WKB method of [21] for the solution of the Fokker-Planck equation for the probability density function. Our main analytical result is the calculation of the probability density function of the local fluctuations near the nonequilibrium steady state, in Sec. IV. In Sec. V we present a numerical solution of the eikonal (Hamilton-Jacobi) equation by the method of characteristics. This equation results from the WKB solution presented in Sec. III. We compare the asymptotic results of Sec. III with the numerical solution and determine the range of their validity. Finally, Sec. VI concludes with a discussion of the results and with comments about future directions.

II. THE UNDERDAMPED PHYSICAL PENDULUM

The underdamped forced physical pendulum is a classical example of a nonlinear multistable dynamical system. It has both stable equilibria and a nonequilibrium stable steady state. Specifically, the equation of motion is given by

$$M\ddot{\theta}+\gamma\dot{\theta}+mgl\sin\theta=\tau, \tag{2.1}$$

where m is the mass of the pendulum M is its moment of inertia, l is the distance between the center of mass and the axis of rotations, γ is a friction coefficient, τ is the external torque, and θ is the angle relative to the equilibrium state of the pendulum. Another physical realization which was widely studied during the past years is the shunted Josephson junction. This system is described by the phenomenological equations [23,24,34]

$$C\frac{dV}{dt}+\frac{V}{R}+I_J\sin\theta=I_{\rm dc}\ . \tag{2.2}$$

Here, C is the capacitance, R is the resistance, I_J is the Josephson critical current, $I_{\rm dc}$ is the external dc current source, V is the voltage across the junction, and θ is the superconducting phase difference across the junction. The Josephson relation between V and θ is $\dot\theta=2eV/\hbar$.

Both systems can be written in the dimensionless form

$$\ddot x+G\dot x+\sin x=I\ . \tag{2.3}$$

For the physical pendulum, G and I are given by

$$G=\gamma\sqrt{mgl/M}\ ,\quad I=\frac{\tau}{mgl}\ , \tag{2.4}$$

and time is the measured in units of $\sqrt{M/mgl}$. For the Josephson junction

$$G=\frac{1}{\omega_J RC}\ ,\quad I=\frac{I_{\rm dc}}{I_J}\ ,\quad \omega_J^2=\frac{2eI_J}{\hbar C}\ , \tag{2.5}$$

and time is measured in units of $1/\omega_J$.

Equation (2.3) also describes the motion of a particle of unit mass in a "washboard" potential field $U(x)=-\cos x-Ix$ (Fig. 1). In phase space, Eq. (2.3) is written as the dynamical system

$$\dot x=y,\quad \dot y=-Gy-U'(x)\ . \tag{2.6}$$

The dynamics of the system depends on the value of the dimensionless coefficients G and I. If $I>1$, the potential $U(x)$ has no local minima, hence there is no equilibrium solution to (2.6). The only asymptotically stable solution then is a steady periodic state S, where the particle moves down the potential with a periodically varying velocity whose time average in the limit $G/I\ll 1$ is given by $\langle\dot x\rangle=I/G$. This steady-state trajectory, $y_S(x)$, can be expanded as a series in powers of G/I,

$$y_S(x)=\frac{I}{G}+\frac{G}{I}\cos\left[x+\frac{G^2}{I}\right]-\frac{1}{4}\left[\frac{G}{I}\right]^3\cos 2x+O\left[\left[\frac{G}{I}\right]^5\right]\ . \tag{2.7}$$

If $I<1$, the points $x=x_E\equiv\sin^{-1}(I)+2\pi n$, $y=y_e\equiv 0$ are equilibrium states and are denoted by E. For values of G below a critical value $G_c(I)$, both equilibrium and hysteretic nonequilibrium steady states can coexist, so that the system is multistable (Fig. 2). In this parameter regime, the phase space is divided into a basin of attraction D_S of the stable nonequilibrium steady state S, and basins of attraction D_E and each of the stable equilibrium states E (see Fig. 2). The basins are separated from each other by *separatrices*, which correspond to solutions of (2.6) that pass through the saddle points C, defined by $x_C=-\sin^{-1}(I)+2\pi(n+\frac{1}{2})$, $y_C=0$ $(n=0,\pm1,\ldots)$ [the local maxima of $U(x)$].

The function $G_c(I)$ represents the maximal value of G for which the system is multistable for a given value of I. If $G=G_c$, each separatrix passes through two saddle points, corresponding to the motion where the particle is initially at rest at a maximum of $U(x)$, and approaches asymptotically the next maximum. As was shown in [21], for small I, $G_c(I)$ is given approximately by

$$G_c(I)\simeq\frac{\pi}{4}I\ . \tag{2.8}$$

For a given G, we define the corresponding value of I, denoted by $I_{\rm min}(G)$, for which $G_c(I_{\rm min})=G$. In Fig. 3, we show the calculated function $I_{\rm min}(G)$. To calculate $G_c(I)$ numerically, we integrated Eq. (2.6) backwards in time, starting from the saddle point C for a given I, looking for the value of G for which the solution will intersect the previous saddle point.

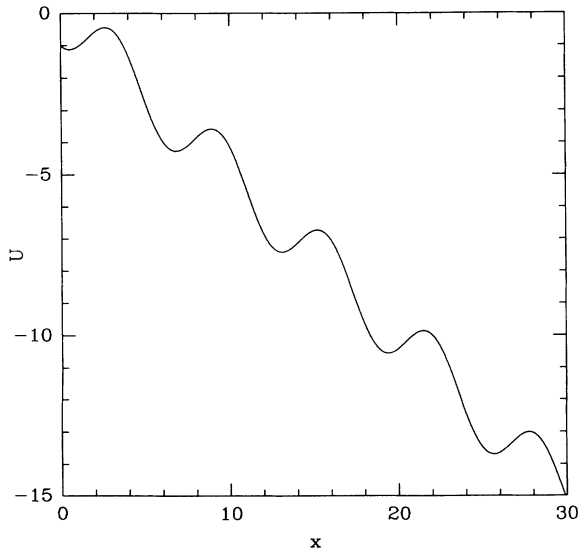

FIG. 1. The potential $U(x)=-Ix-\cos x$ for $I<1$.

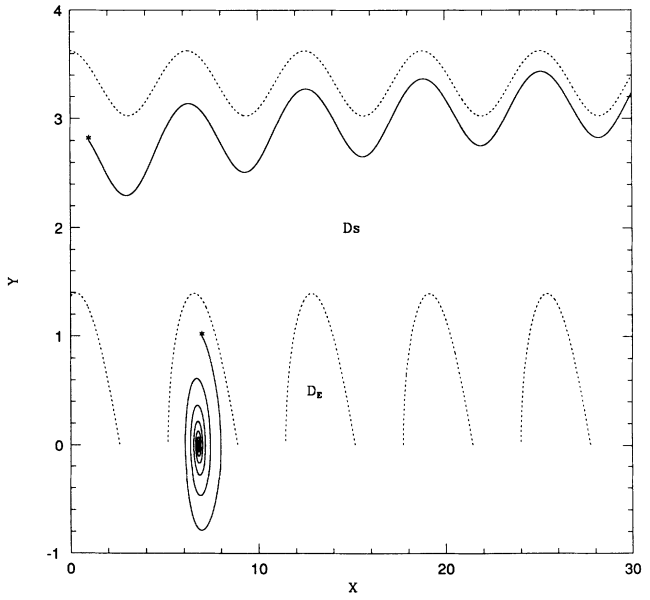

FIG. 2. Trajectories in phase space. Top: A trajectory inside D_S. (2) Bottom: trajectory inside D_E.

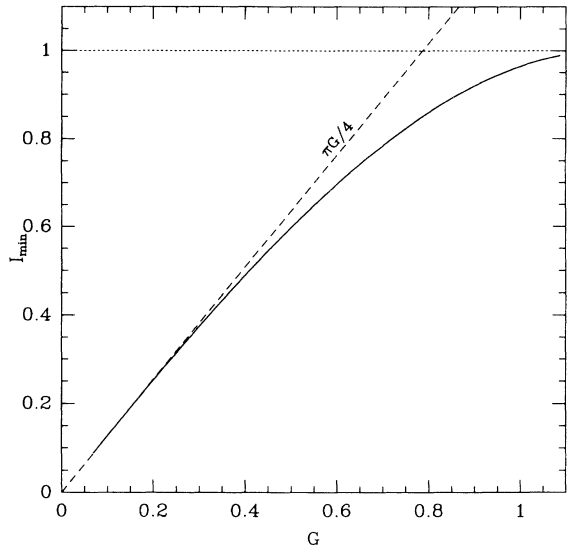

FIG. 3. The function $I_{\min}(G)$ (solid line). (2.8) (dashed line).

III. PROBABILITY DENSITY OF FLUCTUATIONS IN THE PRESENCE OF THERMAL NOISE

We now consider the effect of thermal (Johnson) noise on the dynamics of the pendulum described in the preceding section. Following [21,35], we assume a Langevin model

$$\ddot{x}+G\dot{x}+U'(x)=L(t)\ , \tag{3.1}$$

where $L(t)$ is a standard Gaussian white noise satisfying

$$\langle L(t+s)L(t)\rangle=2GT\delta(s)\ , \tag{3.2}$$

and T is the dimensionless temperature in units of a characteristic temperature ϵ/k_B. For the physical pendulum,

$$\epsilon=mgl\ , \tag{3.3}$$

and for the Josephson junction

$$\epsilon=E_J\equiv\frac{\hbar I_J}{2e}\ . \tag{3.4}$$

Next, we discuss the justification of considering the Johnson noise as the main contribution to thermal noise in the Josephson junction. Shot noise [32,37] can be neglected if $eV<k_BT$. In terms of dimensionless units, this means that

$$\frac{I}{G}<\frac{2E_J}{\hbar\omega_J}T\ , \tag{3.5}$$

where the ratio $E_J/\hbar\omega_J$ is much larger than one, if quantum effects are negligible [15,32]. As shown in Sec. IV, the WKB approximation which is used below is valid if

$$T<W_{\max}\approx\frac{1}{2}\left[\frac{I}{G}\right]^2\ . \tag{3.6}$$

The conditions (3.5) and (3.6) are satisfied if

$$\frac{G}{I}<\frac{E_J}{\hbar\omega_J}\ . \tag{3.7}$$

The condition for multistability in the system is that $G/I<1$, hence (3.7) can be satisfied whenever the system is classical and multistable. Thus multistability corresponds to an underdamped pendulum (see discussion of this point in Sec. VI).

The distribution of fluctuations of the stochastic system (3.1) is determined by a probability density function $p(x,y,t)$, which is a solution of the Fokker-Planck equation [21]

$$\frac{\partial p}{\partial t}=-y\frac{\partial p}{\partial x}+U'(x)\frac{\partial p}{\partial y}+G\frac{\partial}{\partial y}\left[yp+T\frac{\partial p}{\partial y}\right]\ . \tag{3.8}$$

When the system (2.6) is (multi)stable, Eq. (3.8) has a stationary solution $p(x,y)$, which is a 2π-periodic function of x. $p(x,y)$ is well approximated inside D_E by the unnormalized Boltzmann density function

$$p_B(x,y)=e^{-E/T}\ , \tag{3.9}$$

where $E\equiv y^2/2+U(x)$ is the energy. However, $p_B(x,y)$ cannot describe the stationary solution of Eq. (3.8) in D_S, since it is not a 2π-periodic function of x.

For low temperature we assume the WKB approximation for $p_S(x,y)$ in D_S [21]

$$p_S(x,y)=p_0(x,y)e^{-W(x,y)/T}\ , \tag{3.10}$$

where $W(x,y)$ is a solution of the Hamilton-Jacobi-(eikonal-) type equation

$$\mathcal{F}(x,y,W_x,W_y,W)\equiv GW_y^2+yW_x-[Gy+U'(x)]W_y=0 \tag{3.11}$$

(here subscripts denote partial differentiation). The preexpotential factor $p_0(x,y)$ is assumed to have a regular asymptotic expansion in powers of T,

$$p_0(x,y)\sim p^0(x,y)+Tp^1(x,y)+\cdots\ . \tag{3.12}$$

The leading term $p^0(x,y)$ is a solution of the transport equation

$$y\frac{\partial p^0}{\partial x}+[2GW_y-G_y-U'(x)]\frac{\partial p^0}{\partial y}+G(W_{yy}-1)p^0=0\ . \tag{3.13}$$

The parametric equations for the constant W contours are

$$\begin{aligned}\dot{x}&=y\ ,\\ \dot{y}&=-Gy-U'(x)+GW_y\ .\end{aligned} \tag{3.14}$$

It was shown in [21] that for a rotating underdamped forced pendulum, we have on each W contour, given by $y=y_W(x)$,

$$W_y(x,y_W(x))=y_W(x)K(W)+O(G^2)\ , \tag{3.15}$$

where $K(W)$ is constant on the contour. Hence Eq. (3.14) is asymptotically identical to Eq. (2.6), except that G has been replaced by Γ, where

$$\Gamma \equiv G[1-K(W)] \ . \tag{3.16}$$

We denote by $W(\Gamma)$ the value of W corresponding to a given value of Γ, and by $\Gamma(W)$ the value of Γ corresponding to a given value of W in (3.16) (Fig. 4). This means that the W contours correspond approximately to the nonequilibrium steady-state trajectories of the noiseless system (2.6), with G replaced by Γ, for $0<\Gamma<G_c(I)$. The function $W(x,y)$ is constant on the 2π-periodic trajectory $y_\Gamma(x)$ defined by (3.14) with G replaced by Γ only in the limit $\Gamma/I \to 0$. For finite, though small values of $\Gamma/I \ll 1$, the asymptotic expansion of $W(x,y_\Gamma(x))$ is given by

$$W(x,y_\Gamma(x)) \sim \int_G^\Gamma y_\Gamma^2(x)\left[\frac{1}{G}-\frac{1}{\Gamma}\right]d\Gamma \ , \tag{3.17}$$

where $y_\Gamma(x)$ is given by (2.7) with G replaced by Γ. For $\Gamma/I \ll 1$ we obtain

$$W(x,y_\Gamma(x)) \sim W(\Gamma) \sim \frac{1}{2}\left[\frac{I}{G}-\frac{I}{\Gamma}\right]^2 \tag{3.18}$$

(see the Appendix for an explicit derivation). The asymptotic expansion of the leading term $p^0(x,y)$ in (3.12) is given by

$$p(x,y)=1+O(G^2) \ . \tag{3.19}$$

It follows that the stationary probability density of fluctuations about S is given by

$$p_S(x,y) \sim \exp\left[-\left[\frac{I}{G}-\frac{I}{\Gamma}\right]^2/2T\right] \ . \tag{3.20}$$

Note that Γ depends on the point (x,y), since it is defined by (3.16) with $W=W(x,y)$.

The result (3.20) can be expressed in terms of a generalized action. We define the action of the motion on the trajectory $y=y_\Gamma(x)$ by

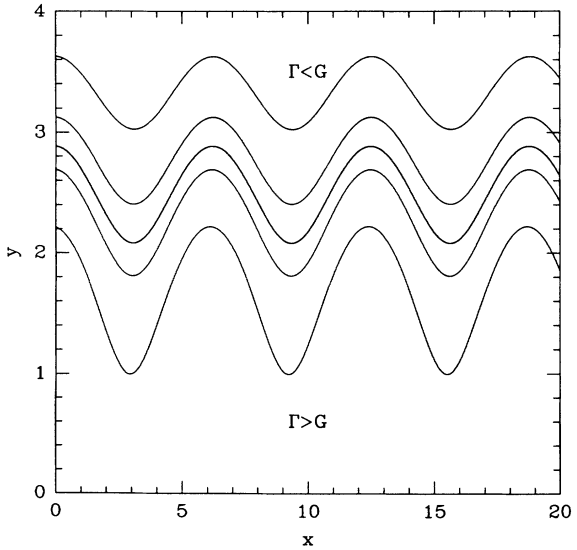

FIG. 4. Constant W contours for various values of Γ.

$$A(\Gamma) \equiv \frac{1}{2\pi}\int_0^{2\pi} y_\Gamma(x)dx \sim \frac{\Gamma}{I} \quad \text{for } \frac{\Gamma}{I} \ll 1 \ , \tag{3.21}$$

and set $A(G) \equiv A_0$, so that Eq. (3.20) can be written as

$$p_S(x,y) \simeq \exp\left[-\frac{[A(\Gamma)-A_0]^2}{2T}\right] \ . \tag{3.22}$$

Thus constant W contours are asymptotically contours of constant A. We use (3.22) below to calculate the mean lifetime of the nonequilibrium steady state. Since the system is underdamped and $p_S(x,y)$ is almost constant on each W contour, the Fokker-Planck equation (3.8) can be average on W contours [21] to yield a one-dimensional Smoluchowski-type equation, which describes diffusion in the action space

$$\frac{\partial p}{\partial t} = G\frac{\partial}{\partial A}\left[[A(\Gamma)-A_0]p + T\frac{\partial p}{\partial A}\right] \ . \tag{3.23}$$

Equation (3.23) is analogous to Kramers's averaged equation for the probability density function of an underdamped system in D_E. It follows that the transition rate from D_S to D_E is given by Kramers's formula for the underdamped regime. Therefore, using the inverse proportionality between the current density and the mean lifetime τ_s, we find

$$\tau_s \simeq \frac{\sqrt{\pi}}{G}\left[\frac{T}{\Delta W}\right]^{1/2}\exp\left[\frac{\Delta W}{T}\right] \ , \tag{3.24}$$

where ΔW is the increment in W between S and the W contour that touches the separatrix. The value of W on S is constant, which we take to be zero [21]. The W contour that first touches the separatrix is given by $W=W_{\max}$, so that $\Delta W = W_{\max}$. This contour touches the separatrix approximately at the unstable equilibrium point C. Using (3.17) and (2.8) we find the asymptotic approximation

$$\Delta W = W_{\max} \simeq \frac{1}{2}\left[\frac{I}{G_c(I)}-\frac{I}{G}\right]^2 \ . \tag{3.25}$$

The expression (3.24) is similar to the Arrhenius factor which characterizes the mean escape time from a harmonic potential well in action space.

In the next sections we describe a numerical procedure to solve Eq. (3.11), and compare the numerical results with the above analytic approximations.

IV. LOCAL FLUCTUATIONS NEAR THE STEADY-STATE SOLUTION

In this section we study the probability density function $p_S(x,y)$, given by (3.20), locally near S by constructing an expansion of W near the steady-state trajectory $y_S(x)$, and describe the local fluctuations about it. In Sec. V this expansion is used to provide the initial conditions for the numerical calculation of W throughout D_S.

The local expansion is given in terms of the local coordinates (x,δ) (see Fig. 5), where

$$\delta \equiv y_S(x)-y \ .$$

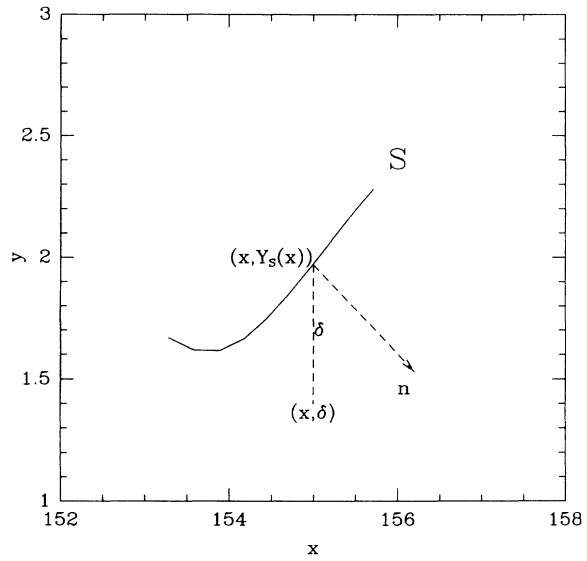

FIG. 5. Local coordinates near S.

It was shown in [21] that on the steady-state trajectory $y_S(x)$, the solution of Eq. (3.11) satisfies

$$W(x,y_S(x))=W_x(x,y_S(x))=W_y(x,y_S(x))=0 . \tag{4.1}$$

Hence Taylor's expansion of $W(x,y)$ in powers of δ is given by

$$W(x,y)=\tfrac{1}{2}\alpha(x)\delta^2+\tfrac{1}{6}\beta(x)\delta^3+\cdots , \tag{4.2}$$

where $\alpha(x),\beta(x)\ldots$, are yet undetermined functions. It follows that Taylor's expansions of $W_x(x,y)$ and $W_y(x,y)$ are given by

$$W_x(x,y)=-\frac{n_x(x,y)}{n_y(x,y)}\alpha(x)\delta + \frac{1}{2}\left[\alpha'(x)-\frac{n_x(x,y)}{n_y(x,y)}\beta(x)\right]\delta^2+\cdots \tag{4.3}$$

and

$$W_y(x,y)=\alpha(x)\delta+\tfrac{1}{2}\beta(x)\delta^2+\cdots . \tag{4.4}$$

The functions $n_x(x,y)$ and $n_y(x,y)$ are the components of the unit normal vector $\mathbf{n}$ to S at $(x,y_S(x))$ (see Fig. 5). The vector $\mathbf{n}$ is orthogonal to the vector $(y_S(x),-Gy_S(x)-U'(x))$, which defines the flow (2.6). Hence

$$n_x(x,y)=\frac{-[Gy_S(x)+U'(x)]}{\{y_S(x)^2+[Gy_S(x)+U'(x)]^2\}^{1/2}} , \qquad n_y(x,y)=\frac{-y_S(x)}{\{y_S(x)^2+[Gy_S(x)+U'(x)]^2\}^{1/2}} . \tag{4.5}$$

We substituted the expansions (4.3) and (4.4) of W_x and W_y in the Hamiltonian-Jacobi equation (3.11) to get

$$\frac{\delta}{n_y(x,y)}[\alpha(x)+\tfrac{1}{2}\beta(x)\delta]\{n_y(x,y)[Gy_S(x)+U'(x)]-n_x(x,y)y_S(x)\} +\delta^2\left[\frac{1}{2}\alpha'(x)y_S(x)+\left[-\frac{n_x(x,y)}{n_y(x,y)}-G\right]\alpha(x)+G\alpha^2(x)\right]=O(\delta^3) . \tag{4.6}$$

The expression in the curly brackets in the first term vanishes, since it is the scalar product of the flow and its normal $\mathbf{n}$. Note that the function $\beta(x)$ is no longer needed for the calculation of $\alpha(x)$. It follows that $\alpha(x)$ satisfies the Bernoulli equation

$$\tfrac{1}{2}\alpha'(x)y_S(x)+\left[-\frac{n_x(x,y)}{n_y(x,y)}-G\right]\alpha(x)+G\alpha^2(x)=0 . \tag{4.7}$$

We first convert (4.7) into a linear equation by the substitution

$$\alpha(x)\equiv\frac{1}{A(x)} \tag{4.8}$$

to get

$$A'(x)-r(x)A(x)=t(x) . \tag{4.9}$$

Here, the coefficients are given by

$$r(x)\equiv\left[\frac{n_x(x,y)}{n_y(x,y)}-G\right]\Big/[\tfrac{1}{2}y_S(x)]=\frac{2U'(x)}{y_S^2(x)} , \tag{4.10}$$

and

$$t(x)\equiv\frac{2G}{y_S(x)} . \tag{4.11}$$

The 2π-periodic solution of (4.9) is

$$A(x)=\frac{1}{R(x)}\left[\frac{\int_0^{2\pi}t(z)R(z)dz}{1-R(0)}R(0)+\int_0^x t(z)R(z)dz\right] , \tag{4.12}$$

where

$$R(z)\equiv\exp\left[\int_z^{2\pi}r(u)du\right] . \tag{4.13}$$

Next, we discuss the local fluctuations about $y_S(x)$. The function $\alpha(x)$ is the local frequency of the quasipotential $W(x,y)$ in the y direction. In the limit $G/I\ll 1$, the variance of the local fluctuations of y, at fixed x, is given by

$$\sigma_y^2(x)=\frac{\int\delta^2\exp[-\tfrac{1}{2}\alpha(x)\delta^2/T]d\delta}{\int\exp[-\tfrac{1}{2}\alpha(x)\delta^2/T]d\delta}=\frac{T}{\alpha(x)} . \tag{4.14}$$

In Fig. 6, we show that the minimum point of $\alpha(x)$ coincides with the point where two neighboring W contours deviate from each other maximally. This point is also the point where $U(x)$ has a local maximum, and $y_S(x)$ has a local minimum.

The average fluctuation of y is given by

$$\sigma_y^2=\frac{\int dx \int \delta^2 \exp[-\frac{1}{2}\alpha(x)\delta^2/T]d\delta}{\int dx \int y \exp[-\frac{1}{2}\alpha(x)\delta^2/T]d\delta}$$
$$=T\frac{\int dx\, \alpha^{-3/2}(x)}{\int dx\, \alpha^{-1/2}(x)} . \tag{4.15}$$

An expansion of $\alpha(x)$ in powers of G/I yields

$$\alpha(x)=1+\left[\frac{G}{I}\right]^2 (I\pi+\cos x)+O\left[\left[\frac{G}{I}\right]^4\right] , \tag{4.16}$$

hence, for $G/I \ll 1$,

$$\sigma_y^2=T\left[1-2\pi\frac{G^2}{I}+O\left[\left[\frac{G}{I}\right]^3\right]\right] . \tag{4.17}$$

These results can be used to calculate the fluctuation in voltage across a Josephson junction for a given current I_{dc}. The voltage is related to the dimensionless velocity by

$$V=I_J R G y , \tag{4.18}$$

hence, using (4.17) and (4.18), and substituting (2.5),

$$\langle \Delta V^2 \rangle=\frac{k_B T'}{C}\left[1-2\pi\frac{G^2}{I}\right]+O\left[\left[\frac{G}{I}\right]^3\right] , \tag{4.19}$$

where T' is the absolute temperature in degrees Kelvin. This fluctuation is a measurable quantity. It corresponds to the width of error bars when measuring the voltage across the junction at a given current I_{dc}.

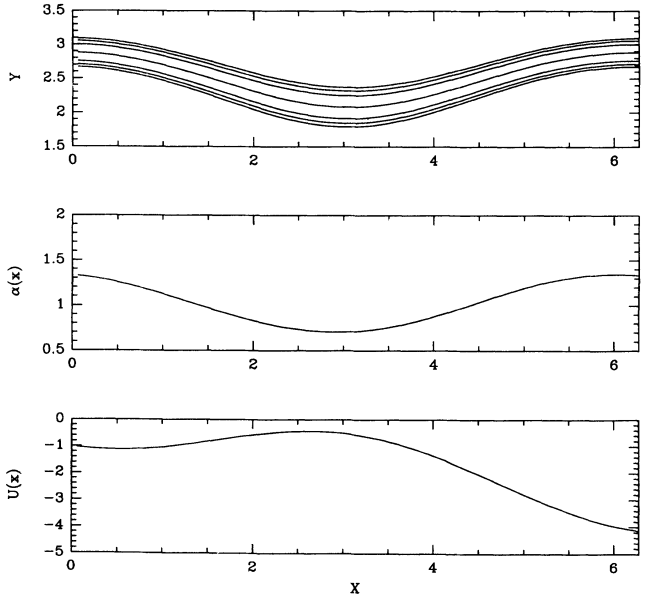

FIG. 6. (a) W contours near $y_S(x)$. (b) $\alpha(x)$. (c) $U(x)$.

V. NUMERICAL SOLUTION OF THE HAMILTON-JACOBI EQUATION

The solution of the Hamilton-Jacobi equation (3.11), which is a 2π-periodic function of x, is constructed by the numerical solution of the characteristic equations [36,37]

$$\dot{x}=\frac{\partial \mathcal{F}}{\partial W_x}=y ,$$
$$\dot{y}=\frac{\partial \mathcal{F}}{\partial W_y}=-Gy-U'(x)+2GW_y ,$$
$$\dot{W}_y=-\frac{\partial \mathcal{F}}{\partial y}-W_y\frac{\partial \mathcal{F}}{\partial W}=-W_x+GW_y , \tag{5.1}$$
$$\dot{W}_x=-\frac{\partial \mathcal{F}}{\partial x}-W_x\frac{\partial \mathcal{F}}{\partial W}=U''(x)W_y ,$$
$$\dot{W}=W_x\frac{\partial \mathcal{F}}{\partial W_x}+W_y\frac{\partial \mathcal{F}}{\partial W_y}=GW_y^2 .$$

The initial conditions for (5.1) are given by Eq. (4.1) on S. However, S is a characteristic curve and a caustic (an attractor of the characteristic curves), so that initial conditions have to be given at a finite distance from S.

We use the expansions (4.2)–(4.4) of W, W_x, and W_y as initial conditions for (5.1) near S. For a given x_0, the value of $y_S(x_0)$ is taken as the approximation (2.7). Then $y_S(x)$ in (2.7) and (4.5) are used to calculate $r(x)$ and $t(x)$ in (4.10) and (4.11), respectively, and $\alpha(x)$ is calculated from (4.8)–(4.13) on a lattice $x_0<x_1<\cdots<x_n=2\pi+x_0$. Although the lattice $(x_i,y_S(x_i)-\delta)$, $i=0,\ldots,n$, which is parallel to the contour $W=0$, could be used for assigning initial conditions, we have chosen the vertical lattice $(x_0,y_S(x_0)-\delta(1+i\Delta))$, $i=1,2,\ldots,k$ for fixed small δ and Δ. We have chosen this lattice rather than a lattice parallel to $y_S(x)$, because the sheaf of characteristics emanating from the vertical lattice covers D_S much more uniformly than the one emanating from the parallel lattice (see Fig. 7). The ini-

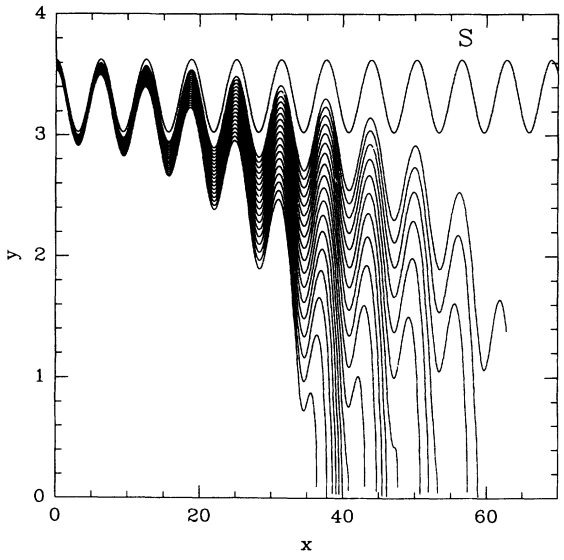

FIG. 7. The characteristic emanating from the running solution.

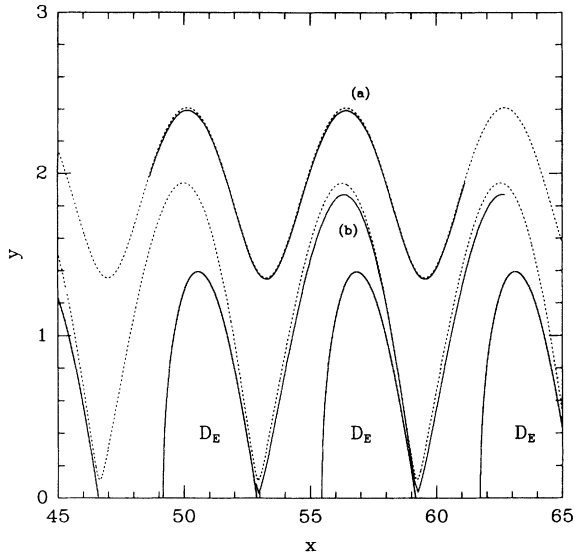

FIG. 8. W contours, (a) $W=1.0$, (b) $W=2.2$ for $G=0.15$ and $I=0.50$. The solid lines are the numerically calculated contours, and the dotted lines are the steady-state solution $y_\Gamma(x)$.

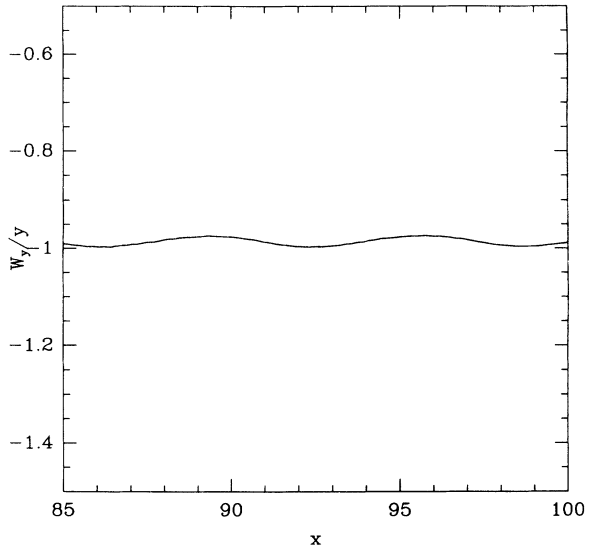

FIG. 10. W_y/y on the contour $W=4.0$ for $G=0.07$ and $I=0.40$. W_{max} is approximately 9.90.

tial values of W, W_x, and W_y are determined on this lattice from (4.2)–(4.4). From each initial point we integrate the characteristic equations (5.1) with the initial conditions (4.2)–(4.4) and construct the W contours with the accumulated data.

Now we describe the results of the numerical solution of (3.11) and compare them with the asymptotic approximation described in Sec. III. We have investigated a wide range of parameters G and I, to check the validity of the three asymptotic approximations: (i) the approximation of the constant W contours by the steady solutions $y_\Gamma(x)$, (ii) the approximation $W_y/y=K(W)+O(G^2)$ (3.15) on a W contour, and (iii) the asymptotic approximation to the exponent ΔW in (3.25).

(i) In Figs. 8 and 9, we see that the W contours coincide very well with $y_\Gamma(x)$ for the contours $W\simeq W_{max}/2$. The maximal relative deviation is less than 1%, and it occurs at the points where the velocity attains its highest value. The deviation becomes more apparent as W approaches W_{max}. For $I=0.5$ (Fig. 8), the maximal relative deviation is less than 5%. However, as I approaches the critical value 1, the approximation breaks down (Fig. 9).

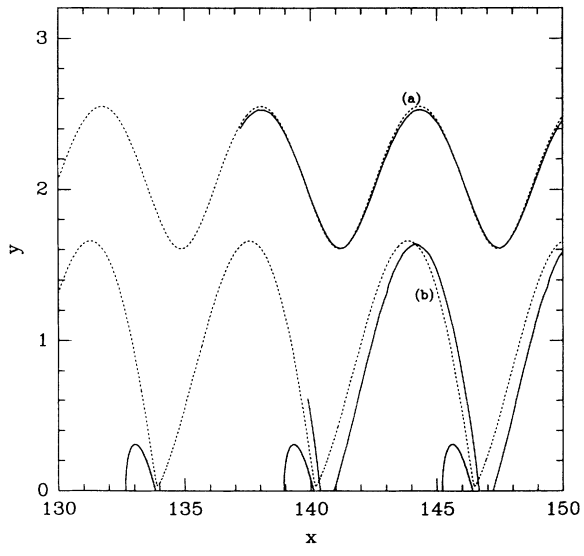

FIG. 9. W contours, (a) $W=3.5$, (b) $W=7.0$ for $G=0.20$ and $I=0.95$. The solid lines are the numerically calculated contours, and the dotted lines are the steady-state solution $y_\Gamma(x)$.

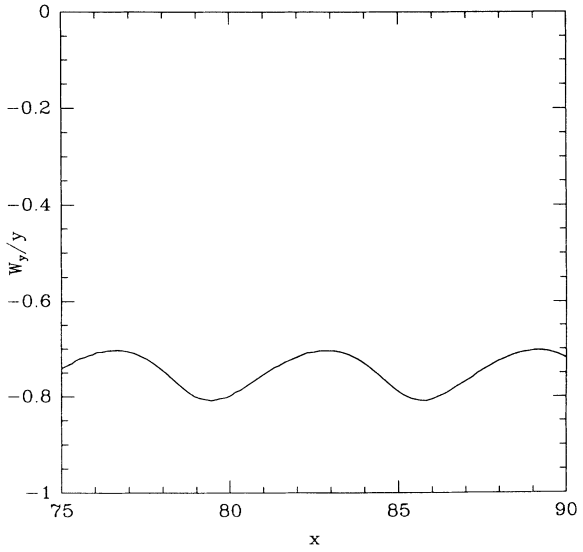

FIG. 11. W_y/y on the contour $W=1.0$ for $G=0.15$ and $I=0.50$. W_{max} is approximately 2.20.

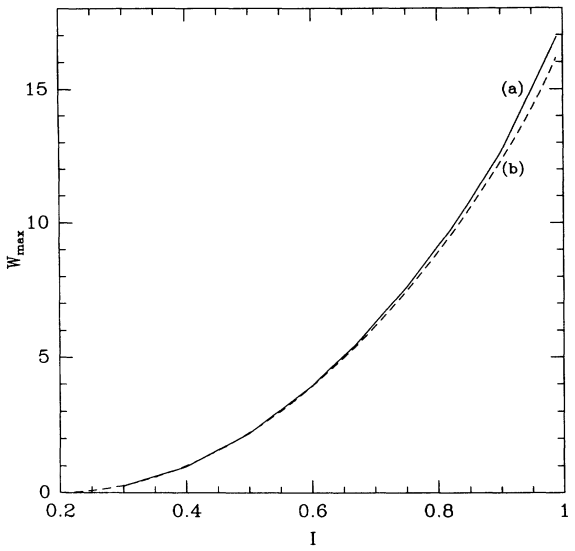

FIG. 12. $W_{max}(I)$ for $G=0.15$: (a) the numerical results; (b) the analytical approximation.

The reason for this breakdown becomes obvious from Fig. 3. As I increases, $G_c(I)$ becomes a nonlinear function, tending asymptotically to infinity at $I=1$. Hence G_c/I exceeds one, and the assumption under which the analytical approximations were derived no longer holds.

(ii) From Figs. 10 and 11, we see that the approximation (3.15) remains accurate only in the limit of small G. The plots of W_y/y versus x on the contour $W \simeq W_{max}/2$ show that W_y/y oscillates with a relative amplitude of about 0.5% for $G=0.07$, and about 7% for $G=0.15$. We note that the approximation (3.15) is the one most sensitive to the condition $G/I \ll 1$.

(iii) In Fig. 12 we see that the approximation (3.25) is very accurate in a wide range of values of I. For $G=0.15$, we find that for $I_{min} < I < 0.8$ the error is less than 2%. This error increase as I approaches 1. However, even very close to 1, it is still less than 10%. For $G=0.5$ (Fig. 13), the error is about 10% for $I_{min} < I < 0.8$, and increase up to 15% for I approaching 1. In this range of parameters the nonequilibrium steady state is very stable, so that the hysteresis is very weak. The lifetime τ_s is in this case extremely long relative to the lifetime of the steady equilibrium state. Thus this range of parameters is of little practical interest for measurements of τ_s. We note that the approximation (3.25) of the height of the effective barrier for the nonequilibrium steady state is robust with respect to G in the range of values where the lifetime τ_s of the state is measurable. This is in spite of the sensitivity of the approximation (3.15), which was used in the derivation of (3.25). We note that τ_s [see (3.24)] is measurable only in a relatively narrow range of the parameters G, I, and T, otherwise being practically infinite. In particular the range of G is limited in the underdamped range.

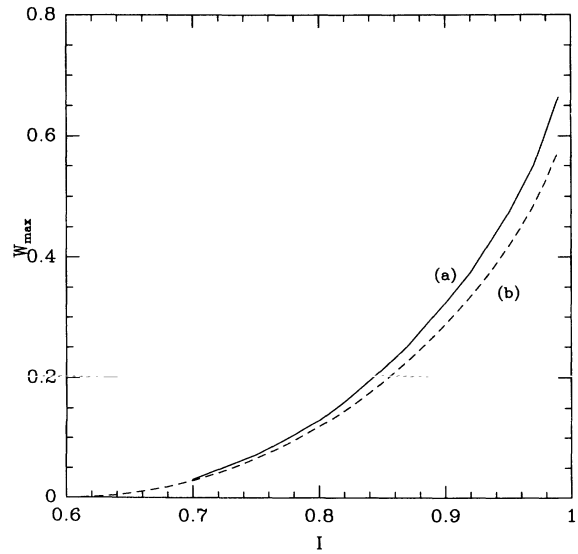

FIG. 13. $W_{max}(I)$ for $G=0.50$: (a) the numerical result; (b) the analytical approximation.

VI. DISCUSSION

The results presented in Sec. V can be interpreted in the context of the shunted Josephson junction. In this system, the nonequilibrium steady state corresponds to the voltage state of the junction, while the equilibrium state is the zero voltage state.

In Sec. V we obtained an approximate expression for the probability density function near the nonequilibrium steady state,

$$p_S(x,y) \simeq \exp\left[-\frac{\alpha(x)[y-y_S(x)]^2}{2T}\right], \tag{6.1}$$

which, in view of (4.18), describes small fluctuations about the voltage state. We found that to leading order of G/I, the average fluctuation in voltage satisfies the relation $C\langle \Delta V^2 \rangle/2 = k_B T'/2$. This means that in the limit of vanishing dissipation, the fluctuations consist only of fluctuations in the charging energy of the capacitor, while the contribution of the Josephson coupling energy is negligible. It is interesting to note that this result coincides with the average fluctuation in voltage about the equilibrium state.

For large fluctuations about the nonequilibrium steady-state trajectory we found that a contour of constant probability coincides approximately with a steady-state trajectory of the noiseless system, corresponding to a certain value of the dissipation coefficient. It was shown in Sec. V that the accuracy of this approximation is within a few percent throughout D_S, as long as I is in the linear part of the graph of the function $I_{min}(G)$ (see Fig. 3), i.e., $I \leq 0.7$. Hence the probability density function of fluctuations is given by

$$p_S(x,y) \simeq \exp\left[-\left[\frac{I}{\Gamma(x,y)}-\frac{I}{G}\right]^2 \Big/ 2T\right], \tag{6.2}$$

where $\Gamma(x,y)$ is the dissipation coefficient corresponding

to the noiseless system whose steady-state trajectory passes through the point (x,y). We note that the exponential factor, which determines the fluctuations near the steady state, depends on the variation in the effective kinetic energy ΔW, unlike the variation in energy, which determines the fluctuations about the equilibrium state.

A reservation about the validity of the approximation of W contours by steady-state trajectories was mentioned in [22]. A discrepancy was point out between the critical contour and the corresponding steady-state trajectory, for the values $I=0.83$ and $G=0.13$. As explained above, this value of I is outside the linear part of the graph of the function $I_{\min}(G)$ (see Fig. 6), so that the condition $G_c(I)/I \ll 1$ is violated, and the approximation breaks down. Nevertheless, we see in Fig. 12 that $W_{\max}$ is still given by this method within an accuracy of a few percent. In the context of the Josephson junction this range of parameters, where the approximation fails, is of no experimental interest, since for usual physical parameters of the junction, the lifetime of the voltage state is practically infinite.

Next, we discuss the lifetime of the nonequilibrium steady state τ_s, which is determined by the critical contour $W=W_{\max}$. Equation (3.25) provides a simple analytic formula for τ_s that can be compared to experiment. The lifetime can be measured by a method similar to that used in the measurement of τ_0, the mean lifetime of the equilibrium state. The system is initialized in the voltage state with $I=I_0>1$. The external current is then decreased at constant rate $\dot{I}$ until transition to the zero voltage state occurs at some $I>I_{\max}(G)$. The transition rate (transition probability per unit time) is $\lambda(I)\equiv\tau_s^{-1}(I)$, with $\lambda(I)=0$ for $I\geq 1$. By repeating this process, the plot of $P(I)$ is obtained, where $P(I)$ is the probability density that transition occurs at current I. The probability density $P(I)$ is related to the mean lifetime $\tau_s(I)$ by

$$P(I)=\frac{1}{\tau_s(I)\dot{I}}\exp\left[-\int_I^1 \frac{dI}{\tau_s(I)\dot{I}}\right], \tag{6.3}$$

hence $\tau_s(I)$ is obtained by inverting Eq. (6.3) numerically.

A second method to measure $\tau_s(I)$ experimentally is given in [19]. In the hysteretic region, the junction jumps between the two states at random times. The mean voltage V, which is directly measurable, is obtained by weighting the two states with their lifetimes τ_0 and τ_s, respectively. Thus

$$V=\frac{0(\tau_0)+V_s(\tau_s)}{\tau_0+\tau_s}, \tag{6.4}$$

where V_s is the voltage in the conducting state. Since τ_0 is given by Kramers's theory, which was confirmed experimentally [38], τ_s can be calculated from (6.4). In [19], the authors took τ_0 to be the transition state theory result [39], and obtained a reasonable agreement between the theoretical and the experimental values of τ_s. The use of (3.24) for the evaluation of τ_s, which corresponds to an underdamped system, and of the transition state theory result for the evaluation of τ_0 in the same system can be understood as follows. As mentioned in Sec. II, the forced pendulum is bistable if it is underdamped. The degree of underdamping for which Kramers's formula (3.24) is valid is different in D_S and in D_E. In D_S (3.24) is valid for most of the range of the parameters G and I for which the system is bistable. In contrast, (3.24) is valid in D_E [with ΔW replaced by $\Delta E_{\max}$, see (6.6)] only if $G \ll T/\Delta E_{\max}$ [40]–[42]. Thus the use of the transition state result for the calculation of τ_0 is justified.

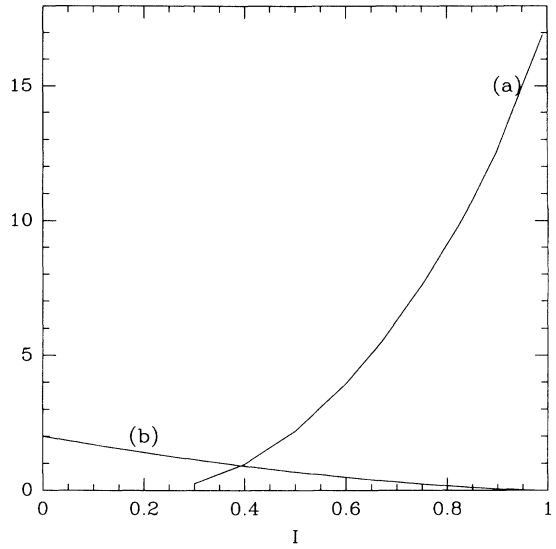

FIG. 14. (a) $W_{\max}(I)$ and (b) $\Delta E_{\max}(I)$ for $G=0.15$.

A measure of the relative stability of the nonequilibrium steady state and the stable equilibrium state is the ratio of their lifetimes, τ_s and τ_0, respectively. We have

$$\lim_{T\to 0} T\ln\frac{\tau_s}{\tau_0}=\Delta W_{\max}-\Delta E_{\max} \tag{6.5}$$

where

$$\Delta E_{\max}=2I\sin^{-1}(I)-\pi I+2(1-I^2)^{1/2} \tag{6.6}$$

is the difference in the potential between the equilibrium state E, and the nearest saddle point C. Therefore we have the asymptotic relation

$$\frac{\tau_s}{\tau_0}\propto\exp\left[\frac{W_{\max}-\Delta E_{\max}}{T}\right]. \tag{6.7}$$

Figure 14 shows plots of $W_{\max}$ and $\Delta E_{\max}$ versus I. Taking, for example, the parameters used in [19], $C=7.2$ nF, $I_J=4\ \mu$A, and $T=4.2$ K, we find that a difference of unity between $W_{\max}$ and $\Delta E_{\max}$ gives a relative stability with an exponential factor of e^{26}, hence the region where the hysteresis can be observed experimentally is very narrow.

ACKNOWLEDGMENTS

We are grateful to D. J. Bergman for useful discussions. This research was partly supported by the Wolfson Foundation through the Israeli Academy of Science.

APPENDIX

We consider the function

$$H(x,y)=\frac{y^2}{2}+U(x) +G\int_{x_0}^{x}[y_\Gamma(\xi)-W_y(\xi,y_\Gamma(\xi))]d\xi\ , \tag{A1}$$

where x_0 is fixed and the integral is taken along the W contour the passes through (x,y). It was shown in [21] that $H(x,y)$ is constant on contours of constant W, so that $H=H(W)$. The rate of change of $H(W)$ on a characteristic curve $(x(s),y(s))$ is given by

$$\frac{d}{ds}H(x(s),y(s))=y(s)\dot{y}(s)+U'(x(s))\dot{x}(s) +G\frac{d}{ds}\int_{x_0}^{x(s)}[y_\Gamma(\xi) -W_y(\xi,y_\Gamma(\xi))]d\xi\ , \tag{A2}$$

where Γ is a function of $(x(s),y(s))$ [the solution of (5.1)]. The derivative of the integral is

$$\frac{d}{ds}\int_{x_0}^{x(s)}(y-W_y)d\xi=\dot{x}(s)[y(s)-W_y(x(s),y(s))] +GW_y^2(x(s),y(s)) \times\int_{x_0}^{x(s)}\frac{1-W_{yy}}{W_y}d\xi\ . \tag{A3}$$

Using this result and (5.1), we find that

$$\frac{d}{ds}H(x(s),y(s))=Gy(s)W_y(x(s),y(s)) +G^2W_y^2(x(s),y(s)) \times\int_{x_0}^{x(s)}\frac{1-W_{yy}}{W_y}d\xi\ . \tag{A4}$$

Now, using (5.1) and (A4), we obtain

$$H'(W)=\frac{dH}{dW}=\frac{\dot{H}}{\dot{W}}=\frac{y}{W_y}+G\int_{x_0}^{x}\frac{1-W_{yy}}{W_y}d\xi\ . \tag{A5}$$

It was shown in [21] that

$$W_{yy}=1+O(G)\ ,$$

hence, on a W contour,

$$W_y(x,y_\Gamma(x))=K(W)y_\Gamma(x)+O(G^2)\ . \tag{A6}$$

Substituting (A6) into the parametric equations (3.14) of the W contours, we see that

$$\dot{x}=y \qquad \dot{y}=-\Gamma y-U'(x)+O(G^3)\ , \tag{A7}$$

where $\Gamma\equiv G(1-K(W))$.

The relation between W and Γ is determined next by the asymptotic relation

$$\Gamma=G\left[1-\frac{W_y(x,y_\Gamma(x))}{y_\Gamma(x)}\right]+O(G^2)\ .$$

On a W contour,

$$\frac{\partial\Gamma}{\partial y}=\left[-\frac{W_{yy}(x,y_\Gamma(x)}{y_\Gamma(x)}+\frac{W_y(x,y_\Gamma(x))}{y_\Gamma^2(x)}\right]+O(G^2) =-\frac{G}{y_\Gamma(x)}\left[\frac{\Gamma}{G}+O(G^2)\right]$$

and

$$\frac{dW}{d\Gamma}=\frac{W_y(x,y_\Gamma(x))}{\partial\Gamma/\partial y}=-\frac{y_\Gamma(x)W_y(x,y_\Gamma(x))+O(G^2)}{\Gamma} =\left[\frac{1}{G}-\frac{1}{\Gamma}\right]y_\Gamma^2(x)[1+O(G^2)] \quad \text{for } \frac{G}{I}\ll 1\ .$$

It follows that

$$W(x,y_\Gamma(x))=\int_G^\Gamma y_\Gamma^2(x)\left[\frac{1}{G}-\frac{1}{\Gamma}\right]d\Gamma+O\left[\frac{\Gamma}{I}\right] \quad \text{for } \frac{\Gamma}{I}\ll 1\ . \tag{A8}$$

For $\Gamma/I\ll 1$, we use (2.7) to write

$$y_\Gamma^2(x)=\frac{I^2}{\Gamma^2}+O\left[\frac{\Gamma}{I}\right]\ ,$$

which gives the approximate solution

$$W(\Gamma)\simeq\frac{1}{2}\left[\frac{1}{G}-\frac{1}{\Gamma}\right]^2 \tag{A9}$$

(see [21]).

[1] H. A. Kramers, Physica **7**, 284 (1940).

[2] R. Landauer and J. A. Swanson, Phys. Rev. **121**, 1668 (1961).

[3] S. Langer, Ann. Phys. (N.Y.) **54**, 258 (1969).

[4] Z. Schuss, SIAM Rev. **22**, 116 (1980).

[5] Z. Schuss, *Theory and Applications of Stochastic Differential Equations* (Wiley, New York, 1980).

[6] N. G. vanKampen, *Stochastic Processes in Physics and Chemistry* (North-Holland, Amsterdam, 1981).

[7] H. Risken, in *The Fokker-Planck Equation,* edited by H. Haken, Springer Series in Synergetics Vol. 18 (Springer, Berlin, 1984).

[8] B. J. Matkowsky, Z. Schuss, and E. Ben-Jacob, SIAM J. Appl. Math. **42**, 835 (1982).

[9] C. W. Gardiner, *Handbook of Stochastic Methods,* 2nd ed. (Springer-Verlag, New York, 1985).

[10] A. Nitzan, Adv. Chem. Phys. **70**, 489 (1987).
[11] M. Büttiker, in *Dynamical Systems: Theory, Experiment, Simulation,* edited by F. Moss and P. V. E. McClintock (Cambridge University Press, Cambridge, England, 1988).
[12] P. Hängii, P. Talkner, and M. Borkovec, Rev. Mod. Phys. **62**, 251 (1990).
[13] T. Naeh, M. M. Klosek, B. J. Matkowsky, and Z. Schuss, SIAM J. Appl. Math. **50**, 595 (1990).
[14] J. Kurkijarvi and V. Ambegaokar, Phys. Lett. **31A**, 314 (1970).
[15] A. J. Leggett, S. Chakravarty, A. T. Dorsey, M. P. A. Fisher, A. Garg, and W. Zwerger, Rev. Mod. Phys. **59**, 1 (1987), and references therein.
[16] J. A. Clarke, N. Cleland, M. H. Devoret, D. Esteve, and J. M. Martinis, Science **239**, 992 (1988), and references therein.
[17] G. R. Fleming and P. G. Wolynes, Phys. Today **43**(5), 36 (1990).
[18] M. Iansiti, M. Tinkham, A. T. Johnson, W. F. Smith, and C. J. Lobb, Phys. Rev. Lett. **59**, 489 (1987); Phys. Rev. B **39**, 6465 (1989); M. Iansiti, A. T. Johnson, C. J. Lobb, and M. Tinkham, *ibid.* **40**, 1370 (1989).
[19] R. Christiano and P. Silvestrini, Phys. Lett. A **133**, 347 (1988).
[20] H. Risken and H. D. Vollmer, Z. Phys. B **33**, 297 (1979); **37**, 343 (1980); **52**, 259 (1983).
[21] E. Ben-Jacob, D. J. Bergman, B. J. Matkowsky, and Z. Schuss, Phys. Rev. A **26**, 2805 (1982).
[22] R. Graham and T. Tél, Phys. Rev. A **33**, 1322 (1986).
[23] W. C. Stewart, Appl. Phys. Lett. **12**, 277 (1968).
[24] D. E. McCumber, J. Appl. Phys. **39**, 3113 (1968).
[25] G. Grüner, A. Zawadowski, and P. M. Chaikin, Phys. Rev. Lett. **46**, 511 (1981).
[26] J. Qui, S. M. Shahidepour, and Z. Schuss, IEEE Trans. Power Appar. Syst. **4**, 197 (1989).
[27] A. Viterbi, *Principles of Coherent Communications* (McGraw-Hill, New York, 1966).
[28] M. Levi, F. C. Hoppenstaedt, and W. L. Miranker, Quart. Appl. Math. **36**, 167 (1978).
[29] Y. Imry and L. Schulman, J. Appl. Phys. **49**, 749 (1978).
[30] E. Ben-Jacob, and D. J. Bergman, Phys. Rev. A **29**, 2021 (1984).
[31] E. Ben-Jacob, D. J. Bergman, Y. Imry, B. J. Matkowsky, and Z. Schuss, J. Appl. Phys. **54**, 6533 (1983).
[32] E. Ben-Jacob, D. J. Bergman, B. J. Matkowsky, and Z. Schuss, Phys. Lett. **99A**, 343 (1983); Ann. N. Y. Acad. Sci. **410**, 323 (1983); E. Ben-Jacob, D. J. Bergman, Y. Imry, B. J. Matkwosky, and Z. Schuss, Appl. Phys. Lett. **42**, 1045 (1983).
[33] E. Ben-Jacob, D. J. Bergman, B. J. Matkowsky, and Z. Schuss, in *SQUID 85,* edited by H. D. Hahlbohm and H. Lübbig (de Gruyter, Berlin, 1985); Phys. Rev. A **34**, 1572 (1986).
[34] L. Solymar, *Superconductive Tunneling and Applications* (Chapman and Hall, London, 1972).
[35] V. Ambegaokar and B. I. Halperin, Phys. Rev. Lett. **22**, 1364 (1969).
[36] R. Courant and D. Hilbert, *Methods of Mathematical Physics* (Wiley-Interscience, New York, 1953).
[37] E. Ben-Jacob, Ph.D. thesis, Tel-Aviv University, 1981.
[38] R. F. Voss and R. A. Webb, Phys. Rev. Lett. **47**, 265 (1981); R. A. Webb, R. F. Voss, and S. M. Faris, *ibid.* **54**, 2712 (1985); S. Washburn, and R. A. Webb, Ann. N.Y. Acad. Sci. **480**, 66 (1986).
[39] S. Glasstone, K. Laidler, and H. Eyring, *The Theory of Rate Processes* (McGraw-Hill, New York, 1966).
[40] V. I. Melnikov and S. V. Meshkov, J. Chem. Phys. **85**, 1018 (1986).
[41] E. Pollak, H. Grabert, and P. Hänngi, J. Chem. Phys. **91**, 4073 (1989).
[42] M. M. Klosek, B. J. Mathkowsky, and Z. Schuss, Ber. Bunsenges. Phys. Chem. **95**(3), 331 (1991).